Crystallization Behavior of Carbon Nanofiber/Linear Low Density Polyethylene Nanocomposites

Sungho Lee,[1,2] Myung-Soo Kim,[3] Amod A. Ogale[1,2]

[1]*Department of Chemical and Biomolecular Engineering, Clemson University, Clemson, SC 29634-0909*
[2]*Center for Advanced Engineering Fibers and Films, Clemson University, Clemson, SC 29634-0909*
[3]*Department of Chemical Engineering, Myongji University, Yongin, Kyunggido 449-728, Korea*

Received 24 February 2007; accepted 20 March 2007
DOI 10.1002/app.26800
Published online 30 July 2007 in Wiley InterScience (www.interscience.wiley.com).

ABSTRACT: Crystallization behavior of LLDPE nanocomposites is reported in the presence of three types of carbon nanofibers (CNFs) (MJ, PR-19, and PR-24). During nonisothermal crystallization studies, all three crystalline melting peaks for LLDPE matrix were observed in the presence of PR-19 nanofibers (up to 15 wt % content), but only the high- and low-temperature peaks were observed in the presence MJ nanofibers. The broad melting peak at low-temperature became bigger, suggesting an increase in the relative content of thinner lamellae in the presence of MJ nanofibers. TEM results of nanocomposites revealed transcrystallinity of LLDPE on the surface of CNFs, and a slightly broader distribution of lamellar thickness. STEM studies revealed a rougher surface morphology of the MJ nanofibers relative to that of PR nanofibers. Also, BET studies confirmed a larger specific surface area of MJ nanofibers relative to that of PR nanofibers, suggesting that the larger and the rougher surface of MJ nanofibers contributes toward the different crystallization behavior of MJ/LLDPE nanocomposites. J Appl Polym Sci 106: 2605–2614, 2007

Key words: polyethylene (PE); nanotechnology; calorimetry; crystallization; TEM

INTRODUCTION

Carbon reinforcements can provide superior electrical conductivity and tensile properties to polymer matrices.[1–5] However, for micro-molding or film applications (product thickness ~ 25 μm), regular carbon fibers cannot be used since the diameter of such fibers is ~10 μm (and length is ~ 100 μm). Instead, nanofibers may be used since the diameter of these nanoreinforcements is only about 0.1 μm. Therefore, recent studies have addressed electrical and mechanical properties of carbon nanotube (CNT) or carbon nanofiber (CNF) reinforced polymer composites.[1–4]

Because of a significantly smaller length scale of nanofibers or nanotubes, crystallization of polymer matrices in the presence of such nanoreinforcements has received significant attention in recent studies.[1,4–7] Lozano and Barrera observed that 5 wt % CNF content led to higher nucleation rate of polypropylene (PP), which reflected as an increase in crystallization temperature by 8°C.[1] It was also observed that the addition of CNT in various polymers such as polyethylene (PE),[3] PP,[4,5] polyvinyl alcohol,[6] and ethylene-vinyl acetate copolymer[7] increased the crystallization temperature without significantly affecting the degree of crystallinity or melting point (T_m). For example, T_m of medium density PE remained almost unchanged after the addition of 10 wt % MWNT (~ 127°C).[3]

Linear low density polyethylene (LLDPE) is widely used for packaging applications because of its film-forming properties, good barrier characteristics, and desirable mechanical properties.[8] These properties of LLDPE can be modified by the incorporation of various α–olefin comonomers such as butene, hexane, and octane.[9] However, incorporation of such comonomers does not appreciably change the electrical properties. Therefore, in this study, CNFs were incorporated into LLDPE to improve electrical conductivity. CNFs were chosen over CNTs because of their lower cost (~ \$0.2/g CNF vs. ~ \$20/g CNT), which is desirable in large-volume applications.

Three different types of CNFs were used for this study: one research grade (MJ) and two commercial grades (PR-19 and PR-24). A typical drop in electrical resistivity was observed for the nanocomposites at the electrical percolation threshold, and the volume resistivity dropped to ~ 9×10^3 ohm cm at about 7.5 vol % MJ nanofibers. PR-24-PS and PR-19-PS nanocomposites displayed a similar electrical behavior, but at slightly higher CNF contents of

Correspondence to: A. A. Ogale (ogale@clemson.edu).
Contract grant sponsor: Engineering Research Center Program, National Science Foundation; contract grant number: EEC-9731680.

TABLE I
Synthesis Conditions and Properties of PR-19, PR-24, and MJ Carbon Nanofibers

	Catalyst	Precursor	Diameter (nm)	Length (μm)	N_2 surface area (m^2/g)
PR-19-PS	Fe-sulfide[a]	Natural gas[a]	100–200[a]	30–100[a]	22
PR-24-PS	Fe-sulfide[a]	Natural gas[a]	60–150[a]	30–100[a]	35
MJ	Ni-Cu[b]	Ethylene gas[b]	50–200[b]	50–100[b]	300

[a] Ref. 11.
[b] Ref. 14.

10 vol %.[10] In this article, we report on the effect of CNFs on the crystallization characteristics of LLDPE, as measured by thermal analysis, wide angle X-ray diffraction (WAXD), and electron microscopy.

EXPERIMENTAL

Materials

Two grades of PyrografIII™ CNFs were obtained from Applied Sciences (Cedarville OH): PR-19-PS and PR-24-PS. These nanofibers were synthesized using the chemical decomposition of methane, ethane, other aliphatic hydrocarbons, or natural gas, which was the primary feed stock, over iron-sulfide catalyst.[11] Both were provided in a pyrolytically stripped (PS) form so that polyaromatic hydrocarbons were removed from the surface. The microstructure and properties of PR-24-PS have been systematically reported by Uchida et al.[12] PR-19-PS nanofibers are otherwise similar to PR-24-PS nanofibers, but have a thin CVD carbon layer deposited as the outer surface.[13] In this article, their designations have been abbreviated as PR-19 and PR-24.

MJ nanofibers represent an experimental grade, and were prepared from the chemical decomposition of ethylene gas over nickel-copper catalyst. MJ nanofibers possessed a twisted or curled microstructure,[14,15] and the details of all three types of CNFs are summarized in Table I.

Poly(ethylene-*co*-1-octene) (DOWLEX 2045 LLDPE, Dow Chemical) used throughout this study is suitable for film applications. The properties of the resin as given by the manufacturer are: density of 0.920 g/cm^3, melt flow index (MFI) of 1.0 g/10 min, DSC melting point of 122°C, and Vicat softening point of 108°C.

Rheomix 600 mixer was used for intensive mixing of LLDPE and various contents of CNFs composites. Thirty grams of physically blended LLDPE and CNFs were fed into the device and mixed for durations ranging from 2 to 20 min at 190°C. Shorter mixing times (2–6 min) resulted in lower percolation threshold and higher electrical conductivity, but also resulted in poorer spatial homogeneity of the nanocomposites. Consequently, a longer mixing time of 20 min was used for all subsequent studies. Next, the compounded forms of pure LLDPE (control) and nanocomposites were pressed in a Carver laboratory press at 190°C at a nominal pressure of 2.8 MPa applied for 5 min. Subsequently, the pressure was increased to 5.5 MPa for 3 min, and pressed samples were air-cooled to ambient conditions in about 10 min.

Carbon nanofiber characterization

The surface area of CNFs was performed by the N_2 adsorption data at 77 K using an automatic surface analyzer (Autosorb-1, Quantachrome Co.). Brunauer-Emmett-Teller (BET) equation was used to quantify surface area of CNFs from gas adsorption isotherms.[16] STEM-Hitachi HD2000 transmission electron microscope (TEM) at 200 kV was used for examining CNFs. Samples were prepared by dispersing CNFs in acetone by sonication for 10 min, and dispensing them on a formvar/carbon film-supported copper grid and dried.

Nanocomposite characterization

Pure LLDPE and its nanocomposites were investigated by WAXD (XDS 2000, Scintag, USA) using Cu–K_α radiation (λ = 1.5406Å) over the 2θ range of 15° to 40°. A scanning rate of 0.02°/s was used for a total exposure time of 20 min per image. Thermal analysis was performed in a Perkin-Elmer Pyris I differential scanning calorimeter (DSC). An indium standard was used for temperature and ΔH calibration. Samples were heated up to 190°C at a rate of 10°C/min and held at that temperature for 10 min to erase prior thermal history of the samples. Subsequently, samples were cooled to 50°C at a rate of 0.5–10°C/min and then heated up to 190°C again at a rate of 10°C/min for studying the effect of nanofibers on nonisothermal crystallization. For isothermal crystallization, samples were rapidly cooled (40°C/min) from 190°C and held at 112–116°C for 60 min.

TEM-Hitachi H 7600 and H 9500 transmission electron microscopes (TEM) were used for investigating crystalline structure of LLDPE in pure and composite forms containing 15 wt % CNFs. To control the thermal history of microscopy samples, they

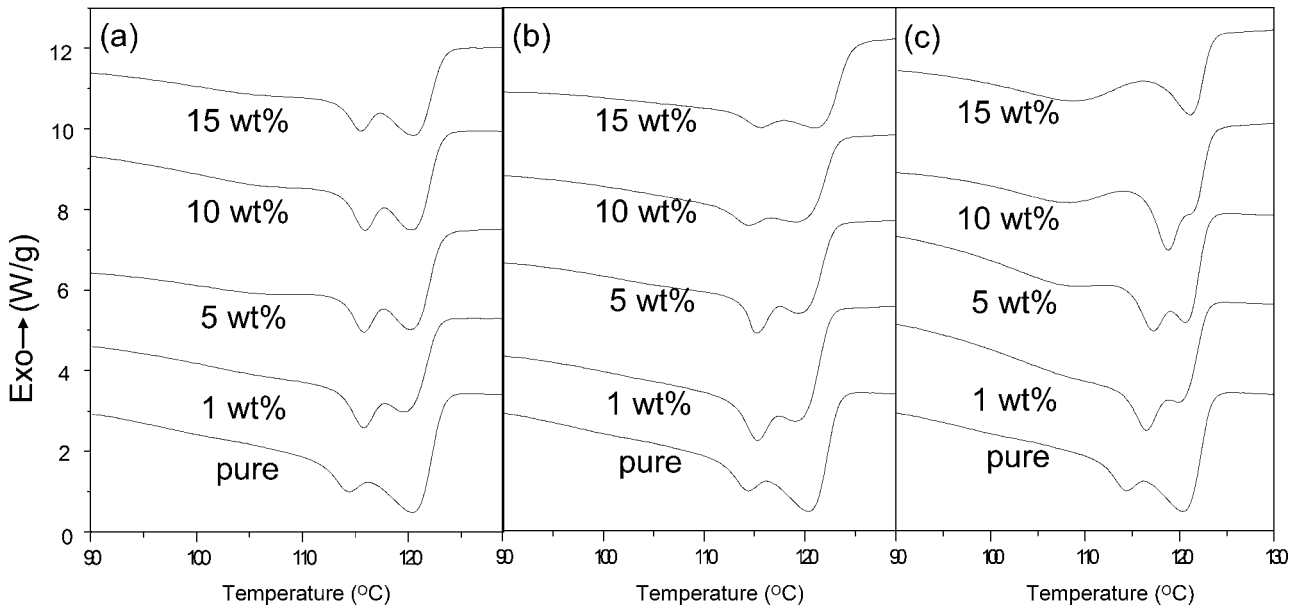

Figure 1 DSC thermograms from first heating at a rate of 10°C/min for pure LLDPE and CNF composites containing: (a) PR-19, (b) PR-24, and (c) MJ CNFs. The baselines are shifted vertically for convenience.

were also processed in the Perkin-Elmer DSC for 10 min at 190°C and cooled down at a rate of 10°C/min. Samples were chemically treated with chlorosulphonic acid for 10 h at 25°C.[17,18] After cryo-microtoming at −50°C, samples were dispensed on a formvar/carbon film-supported copper grid. Subsequently, they were stained with 2% uranyl acetate for 2 h at 25°C.[17,18] The nominal thickness of polymer lamellae was measured in pure LLDPE and 15 wt % CNF nanocomposites. Seven replicate images were obtained for each composition, and the thickness of multiple lamellae (n = 70) was computed by the use of image analysis software provided with the microscope.

RESULTS AND DISCUSSION

Crystallization kinetics

Crystallization behavior of LLDPE in the presence of CNFs was first investigated using nonisothermal DSC analysis, and melting peaks from the first heating scan are displayed in Figure 1(a–c); the baselines are shifted vertically for convenience. Pure LLDPE showed two melting peaks, one at 115°C and the other at 121°C. With the addition of PR-19 and PR-24 CNFs, the melting peaks remained essentially unchanged. But, for MJ nanocomposites, the lower temperature peak (115°C) started to shift to higher temperatures (∼ 120°C), and a broad peak appeared at ∼ 109°C for higher nanofiber contents. Thus, 15 wt % MJ nanocomposite displayed one sharp (121°C) and one broad (∼ 109°C) melting peak.

Since the first heating scans reflect prior thermal history experienced by the nanocomposites during sample processing steps, and may vary from one process to another, second heating scans were also obtained to investigate the crystallization behavior intrinsic to the polymer/CNF material system. Samples were held at 190°C for 10 min after the first heating scan to remove prior thermal history and then cooled at 10°C/min. The cooling crystallization thermograms are presented in Figure 2, followed by the second heating scans at 10°C/min in Figure 3. During cooling, DSC thermograms of pure LLDPE [''pure'' in Fig. 2(a–c)] display one sharp peak at 104.7°C followed by a broad tail (towards lower temperatures). Thermograms for PR nanocomposites, displayed in Figure 2(a,b), also showed a sharp peak and a broad tail with a small shifting of the peak temperature to higher values (104.5 → 106.7°C for PR-19 and 104.5 → 107.9°C for PR-24, as in Table II). In contrast, for MJ nanocomposites, a sharp peak (109.1–113.6°C) and another broad peak (99.5–101.8°C) were observed. It is evident that increasing CNF content shifted the peak temperature of crystallization to significantly higher values, and the broad tail of pure LLDPE became a broad peak.

Thermograms from second-heating are presented in Figure 3, and the measured transition temperatures (T_m) and heats of fusion (ΔH_f) are summarized in Table II. Pure LLDPE displayed melting peaks at three temperatures: 106.5, 118.1, and 122.0°C. For all PR-19 nanocomposites, the three melting peaks were observed with an insignificant increase to higher temperatures. However, for PR-24 nanocomposites, as nanofiber content increased, the meting peaks

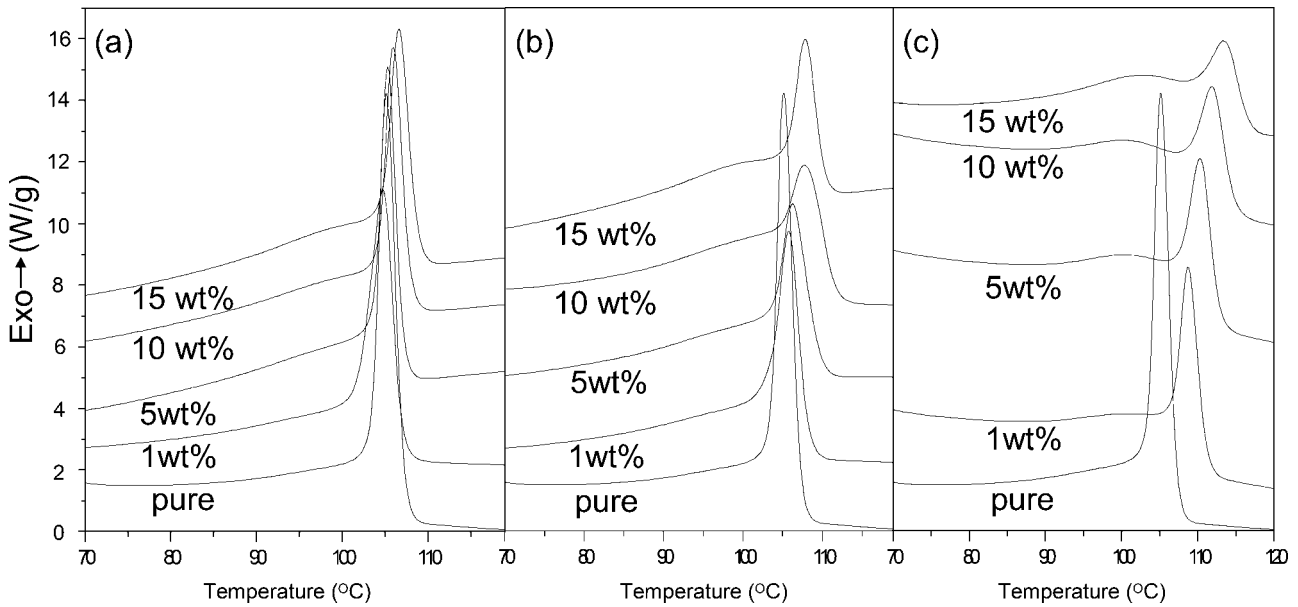

Figure 2 DSC thermograms for cooling at a rate of 10°C/min for pure LLDPE and CNF composites containing: (a) PR-19, (b) PR-24, and (c) MJ CNFs.

shifted to higher temperatures (106.6°C → 108.2°C for the broad peak and 118.5°C → 120.1°C for the sharp peak). Thus, 15 wt% PR-24 nanocomposites showed a broad peak at ~ 108°C and a sharp peak at ~ 120°C.

For 1 wt % MJ nanocomposite, a broad lower melting peak at 109.0°C, a sharper melting peak at 120.6°C, and a shoulder at 122.2°C were observed from Figure 3(c). It is likely that each of the melting peaks of pure LLDPE shifted to higher temperatures with the addition of MJ CNFs. For 5 wt % and higher content of MJ CNFs, two melting peaks were observed in DSC scans: one broad and one sharp. With an increase in CNF content, the broader peak at low temperature gradually became prominent without significant change in peak temperature (~ 109°C). In contrast, the sharp melting temperature increased (120.6°C → 122.4°C) with increasing CNF content.

After deconvolution of DSC thermograms, the relative area under the broad melting peak (109°C) was calculated to be 73.5% ± 1.3%, 72.9% ± 0.3%, 76.9%

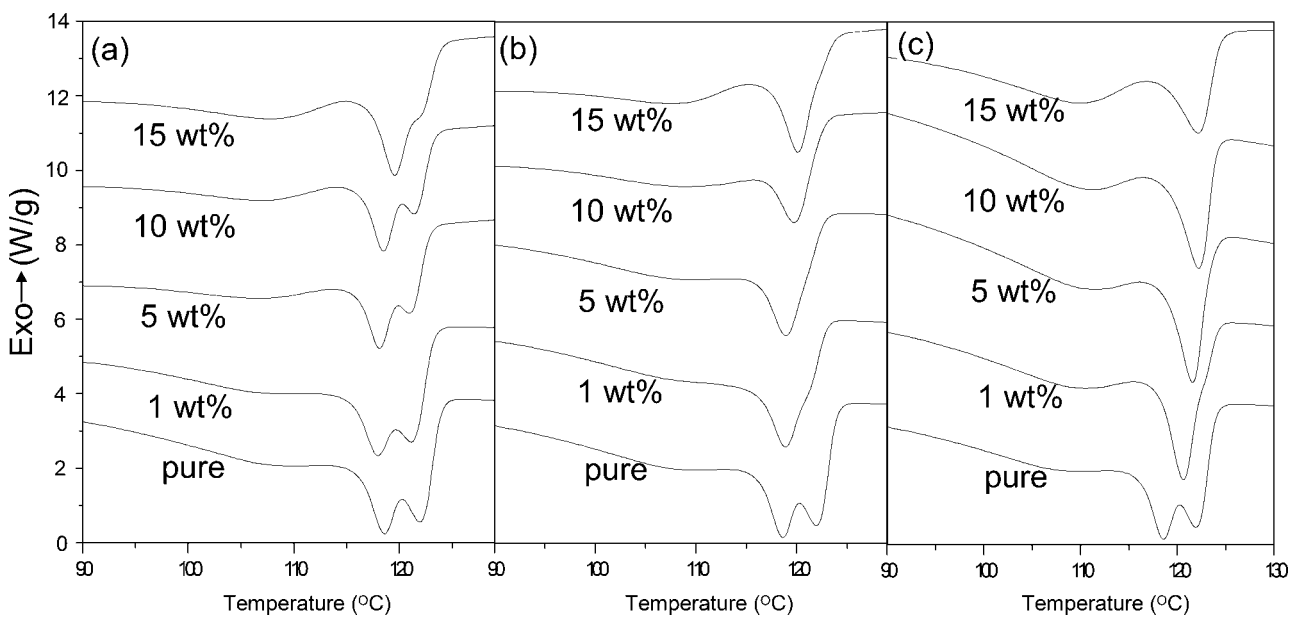

Figure 3 DSC thermograms from second heating at a rate of 10°C/min for pure LLDPE and CNF composites containing: (a) PR-19, (b) PR-24, and (c) MJ CNFs.

TABLE II
The Crystallization Temperatures (T_c), Melting Points (T_m), and Heats of Crystallization Measured by DSC for LLDPE and Its Nanocomposites Containing PR-19, PR-24, and MJ Carbon Nanofibers

Type	CNF content (wt %)	T_{c1} (°C)	T_{c2} (°C)	T_{m1} (°C) (shoulder)	T_{m2} (°C)	T_{m3} (°C)	ΔH_f (J/g_{poly})	X (%)
LLDPE	0	–	104.5 ± 0.3	106.5 ± 1.0	118.1 ± 0.3	122.0 ± 0.2	100.8 ± 1.7	35.0 ± 0.6
PR-19	1	–	104.5 ± 0.3	106.4 ± 0.2	118.0 ± 0.5	121.4 ± 0.2	93.7 ± 1.8	32.5 ± 0.6
	5	–	105.2 ± 0.3	107.1 ± 0.5	118.3 ± 0.2	121.4 ± 0.2	94.5 ± 2.0	32.8 ± 0.7
	10	–	106.3 ± 0.2	107.6 ± 0.2	118.9 ± 0.4	121.9 ± 0.2	94.1 ± 1.6	32.7 ± 0.6
	15	–	106.7 ± 0.2	107.6 ± 0.4	119.2 ± 0.3	122.1 ± 0.1	94.3 ± 1.9	32.7 ± 0.7
PR-24	1	–	105.7 ± 0.1	106.6 ± 0.2	118.5 ± 0.2	Weak shoulder	95.2 ± 1.4	33.0 ± 0.5
	5	–	106.4 ± 0.7	107.4 ± 0.7	119.0 ± 0.4	Weak shoulder	92.1 ± 1.5	32.0 ± 0.5
	10	97.7 ± 0.9	107.9 ± 0.4	108.3 ± 0.2	120.1 ± 0.2	Weak shoulder	97.2 ± 1.6	33.8 ± 0.6
	15	98.2 ± 0.4	107.4 ± 0.4	108.2 ± 0.3	119.7 ± 0.4	Weak shoulder	94.8 ± 1.0	32.9 ± 0.4
MJ	1	99.5 ± 1.0	109.1 ± 0.5	109.0 ± 0.2	120.6 ± 0.1	Weak shoulder	99.3 ± 1.1	34.5 ± 0.4
	5	100.0 ± 0.2	110.3 ± 0.1	109.6 ± 0.2	–	121.4 ± 0.13	99.0 ± 5.1	34.4 ± 1.8
	10	100.4 ± 0.2	112.0 ± 0.1	109.9 ± 0.3	–	122.1 ± 0.12	99.3 ± 1.7	34.2 ± 0.5
	15	101.8 ± 0.1	113.6 ± 0.2	110.2 ± 0.5	–	122.4 ± 0.05	99.3 ± 4.9	33.2 ± 1.7

± 0.2%, and 80.8% ± 0.5% for pure LLDPE, and 1 wt % PR-19, PR-24, and MJ nanocomposites, respectively (Table III). At 15 wt % CNFs, the values were found to be 75.9 ± 1.0, 78.5 ± 0.4, and 83.6 ± 1.1 for PR-19, PR-24 and MJ nanocomposites, respectively (Table III). Representative deconvoluted thermograms for pure LLDPE and 1 wt % and 15 wt % nanocomposites are displayed in Figure 4. These indicate that with increasing CNF content, the broad melting peak became bigger whereas the sharp melting peak became smaller.

It has been reported in the literature that DSC endotherms of LLDPEs prepared by Ziegler-Natta catalyst display multiple melting peaks.[9,19–21] The α–olefin short-chain branches are not introduced at regular intervals in the main LLDPE chain, and the intramolecular and intermolecular heterogeneity leads to multiple melting peaks.[9] The broader melting peak can be attributed to thinner lamellae of highly branched chain segments, whereas the sharper peaks arise from the long thick lamellae containing little or no branches.[9,19–21] Defoor et al. observed by transmission electron microscopy (TEM) that thickest lamellae of LLDPE were mostly formed during the initial stage of the crystallization process.[18] Later, at lower temperatures, thinner lamellae fill up the space between thick lamellae.[18] In addition, depending on the α–olefin used as the comonomer, a broad melting peak with a lower melting point around 106–110°C and higher peaks in the range of 120–124°C have also been observed.[9]

Further, for samples obtained after a slow cooling rate, the disappearance of the sharp melting peak of LLDPE prepared by Ziegler-Natta catalyst systems has been reported in the literature.[9] Even though two sharp melting peaks of these LLDPEs were observed after a fast cooling rate of 10°C/min, only one melting peak appeared after a prior cooling rate of 5°C/min.[9] The double melting peaks (generated during fast-cooling) can be attributed to melt recrystallization, which is the reorganization of meta-stable lamellae into more stable thicker lamellae.[9] A similar melting behavior was observed in Figure 5: for sample cooled at a slow rate of 0.5°C/min, one sharp melting peak was observed, but an additional shoulder appeared in melting peaks for samples that had been cooled at moderate rates of 1°C/min and 2.5°C/min. Further, two distinct melting peaks were observed for samples that had been cooled at the fast rates of 5°C/min and 10°C/min.

For MJ nanocomposites, the 118°C melting peak shifted towards higher temperature, but became smaller. This suggests that CNFs lead to the development of some thicker, but fewer, LLDPE lamellae. However, the observation that the broad melting peak (109°C → 110°C) became bigger with increasing CNF content suggests that CNFs also tend to generate additional thinner LLDPE lamellae. Note that as CNF content increased, the broad peak became more intense in the cooling scan as well [Fig. 2(c)]. It is evident that thin lamellae, likely associated with a broad melting peak in the second heating scan, were formed at lower temperature during cooling with the addition of CNFs.

TABLE III
The Relative Area of Melting Peaks After Deconcolution of DSC Thermograms for LLDPE and Its Nanocomposites Containing PR-19, PR-24, and MJ Carbon Nanofibers

Type	CNF content (wt %)	% Area (T_{m1})	% Area (T_{m2})	% Area (T_{m3})
LLDPE	0	73.5 ± 1.3	14.9 ± 0.4	11.6 ± 1.7
PR-19	1	72.9 ± 0.3	16.2 ± 1.6	10.9 ± 1.3
	15	75.9 ± 1.0	19.5 ± 2.3	4.6 ± 1.7
PR-24	1	76.9 ± 0.2	21.8 ± 0.6	1.4 ± 0.6
	15	78.5 ± 0.4	19.4 ± 0.8	2.1 ± 0.9
MJ	1	80.8 ± 0.5	18.5 ± 0.5	0.7 ± 0.2
	15	83.6 ± 1.1	–	16.4 ± 1.1

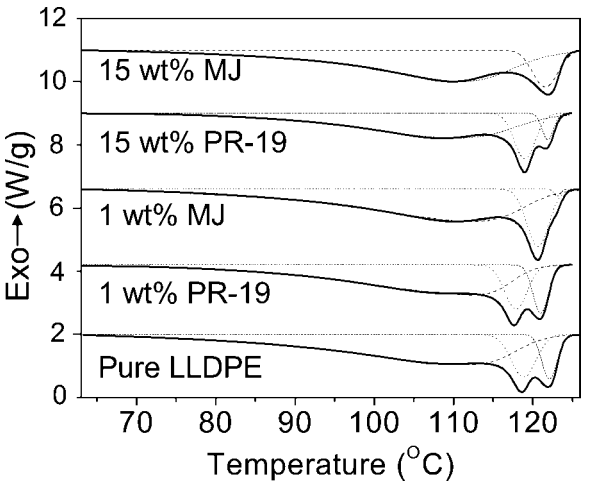

Figure 4 Representative deconvoluted thermograms from second heating cycle of pure LLDPE and CNF nanocomposites.

Nonisothermal crystallization kinetics were studied by nonisothermal Avrami analysis for pure LLDPE and nanocomposites containing 1 wt % of CNFs. The extent of isothermal crystallization, *X(t)*, may be related to time as:

$$1 - X(t) = \exp(-Z_t t^n) \quad (1)$$

where n is the Avrami crystallization exponent, and Z_t is a crystallization rate constant.[22] For nonisothermal crystallization, the modified time t is related to temperature T as $t = (T_o - T)/\phi$ where T_o is the onset temperature of crystallization and ϕ is the cooling rate. From the Avrami plots, n values were calculated to be 2.87 ± 0.01, 2.90 ± 0.11, and 2.83 ± 0.05 for pure LLDPE, 1 wt % PR-19, and 1 wt % PR-24 nanocomposites, respectively. The crystallization exponents for pure LLDPE and PR nanocomposites were statistically not different (at 95% confidence interval). Also, these values were similar to those reported in the literature for polyethylene, a range of 1.7–3.8.[23,24] However, MJ nanocomposite showed two slopes that led to two crystallization exponents: the steeper curve led to values of 2.61 ± 0.03, whereas the shallower curve resulted in 1.13 ± 0.03. It is evident that the second slope resulting from the broad peak (99.5°C) observed in Figure 2(c) indicates slower crystallization.

From the second heating scans, the crystallinity of all samples was determined by dividing ΔH_f of crystallization by ΔH_f^o value of 288 J/g for LLDPE,[25] and the results are summarized in Table II. The normal-

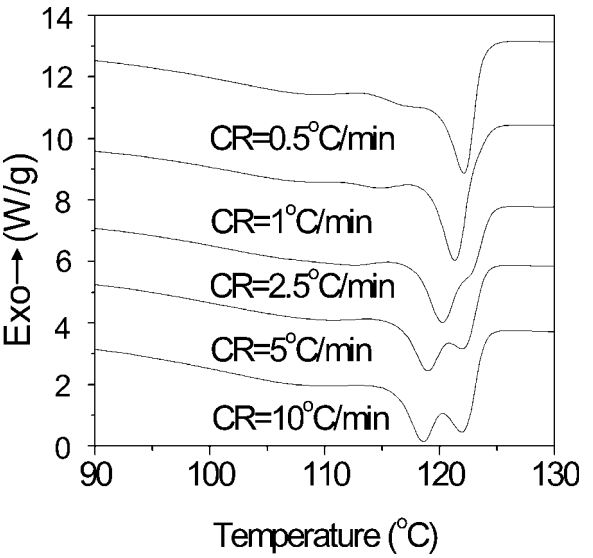

Figure 5 DSC thermograms from second heating cycle at 10°C/min for pure LLDPE samples that had been cooled at various cooling rates (CR).

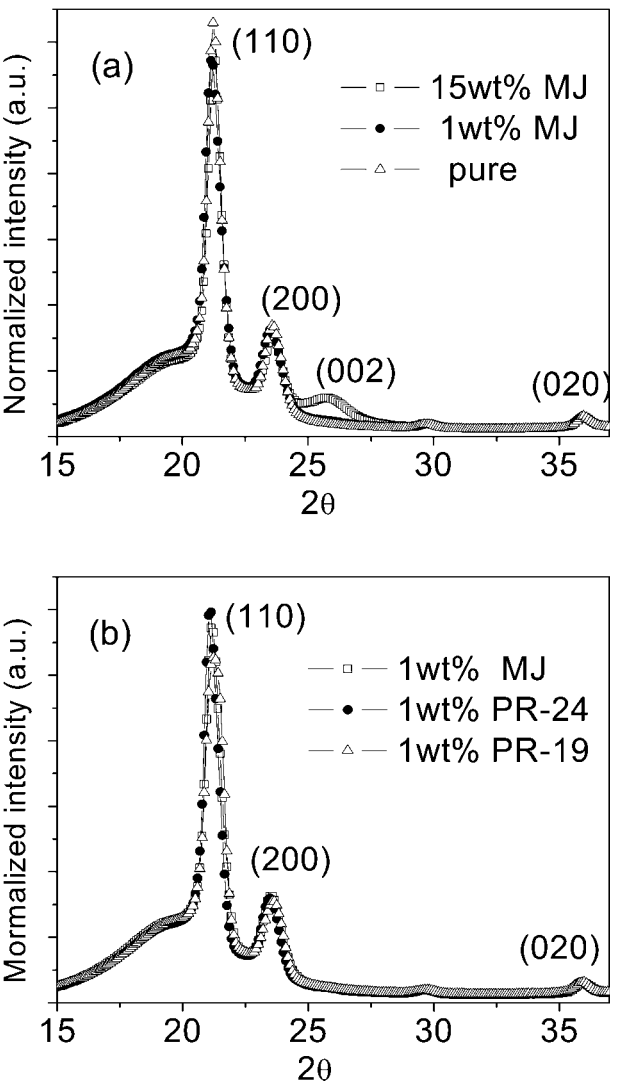

Figure 6 Integrated azimuthal profiles (2θ plots) for: (a) pure LLDPE, and 1 wt % and 15 wt % MJ nanocomposites and (b) 1 wt % nanocomposites containing PR-19, PR-24, or MJ CNFs.

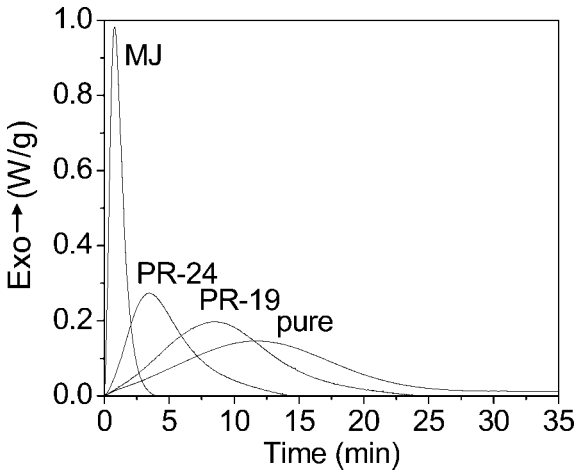

Figure 7 Isothermal crystallization exotherms at 114°C for pure LLDPE, and 1 wt % nanocomposites containing PR-19, PR-24, or MJ CNFs.

ized ΔH_f values reported are based on the polymer content (since fibers do not crystallize). The overall crystallinity of the LLDPE phase for the different samples (35.0–32.7%) did not change significantly with increasing CNF content.

The integrated azimuthal profiles (2θ scans) from WAXD of pure LLDPE, 1 wt % and 15 wt % MJ nanocomposites are displayed in Figure 6(a). The peaks associated with (110), (200), and (020) planes of orthorhombic LLDPE crystals appear at 2θ values of 21.7° ± 0.2°, 24.1° ± 0.2°, and 36.5° ± 0.2°, respectively. For 15 wt % MJ nanocomposites, a peak appears at 2θ ≈ 26° from the (002) graphene planes of CNFs, but the peak positions for LLDPE did not change significantly for any CNF composites. Further, as illustrated in Figure 6(b) for 1 wt % nanocomposites, no measurable change of peak positions was observed with different CNFs. These diffractograms indicates that CNFs did not significantly affect the orthorhombic crystal structure of LLDPE.

Overall crystallinity of LLDPE was also calculated by WAXD in pure polymer samples and those containing 1 wt % CNFs, based on the sum of (110) and (200) peak areas as a ratio of the total area.[26–28] The degree of crystallinity was found to be 36% ± 2%, 34% ± 2%, 34% ± 3%, and 35% ± 2% for pure LLDPE, PR-19, PR-24, and MJ 1 wt % nanocomposites, respectively. These WAXD-based values are consistent with those obtained from DSC (Table II), and indicate that there was not any appreciable difference in the overall degree of crystallinity with the addition of various CNFs.

Isothermal crystallization of pure LLDPE and 1 wt % nanocomposites was conducted in the temperature range from 112°C to 116°C. When samples were quenched to the desired temperature, there was a lag between the sample temperature and programmed temperature. This temperature transience has also been reported in the literature, and is observed due to finite heat capacity of materials and nonisothermal crystallization.[29] Therefore, the initial nonisothermal heat effects are subtracted from the overall heat effects.[29] Corrected isothermal scans,

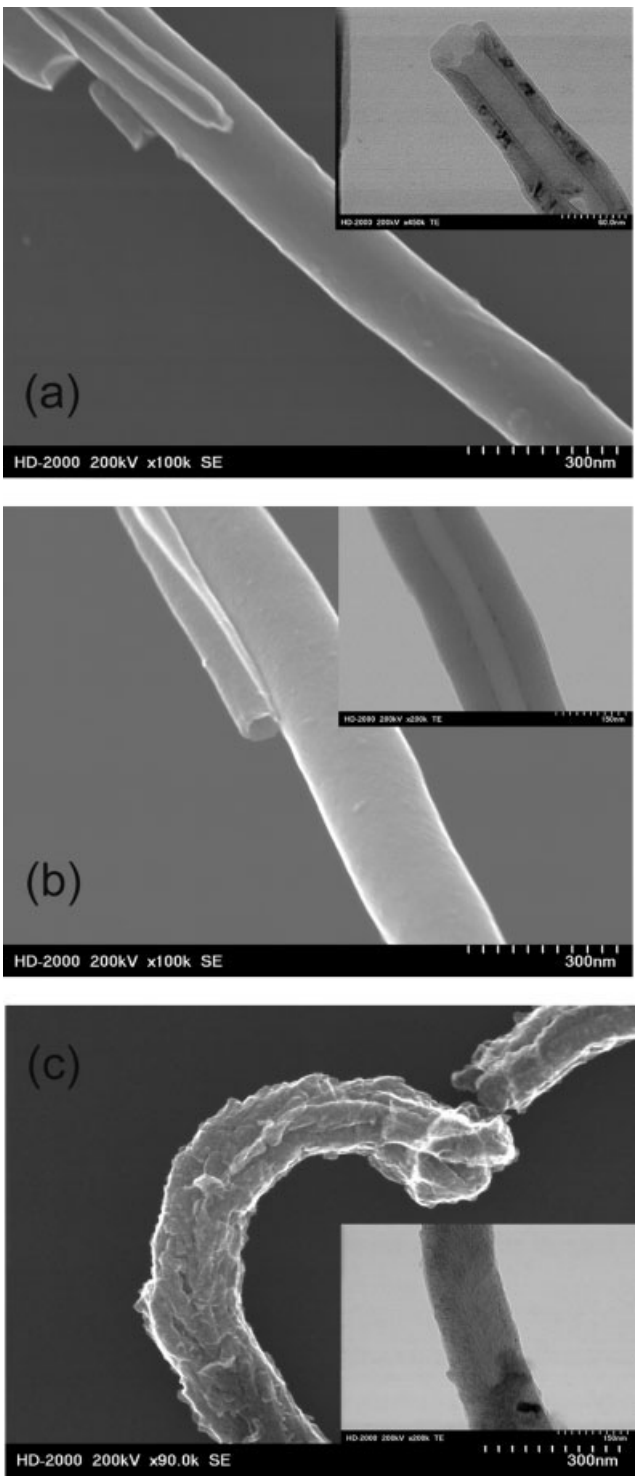

Figure 8 Scanning transmission electron micrographs of: (a) PR-19 (b) PR-24, and (c) MJ CNFs. The inset images are TEM micrographs.

obtained by following this procedure, are displayed in Figure 7. However, due to the removal of initial heat effects, the crystallinity values from isothermal scans are less than those measured from nonisothermal ones. For poly(ethylene-*co*-1-hexane) synthesized by metallocene catalyst, Janimark and Stevens[30] observed that the crystallinity measured from isothermal scans at 110°C was about half of that measured from non-isothermal scans. Since the crystallinity measured from isothermal scans was only about a quarter of that measured from nonisothermal scans in the present study, we believe that these isothermal results do not accurately represent crystallization kinetics.

Fiber structure and LLDPE morphology

To investigate the difference in crystallization kinetics observed with the addition of different nanofibers, microstructural analysis of nanofibers was performed. STEM micrographs for PR-19, PR-24, and MJ nanofibers are presented in Figure 8(a–c), with TEM micrographs shown as insets. The STEM micrographs reveal that the surface of MJ nanofibers was significantly rougher than that of PR-19 and PR-24 nanofibers. The hollow core observed in TEM micrographs for PR-19 and PR-24 nanofibers were consistent with TEM results reported by Uchida et al.[12] and Lakshminarayanan et al.[13] In contrast, a solid core was observed for MJ CNFs, as illustrated by the inset of Figure 8(c). It has been observed in the literature that PR-24-PS nanofibers consist of truncated cones of graphene planes stacked on top of each other to form a single-layer structure.[12] However, in the same grade of PR-24-PS, double-layered structures were also reported in which the inner layer consisted of the stacked truncated cones, whereas the outer layer was oriented along the fiber axis. For PR-19 CNFs, the outer CVD layer will presumably be parallel to the fiber axis, but the presence of such a layer was not clearly seen in the present results.

The specific surface area of the nanofibers was measured by BET measurements, and found to be 22, 35, and 300 m^2/g for PR-19, PR-24, and MJ nanofibers, respectively (Table I). The surface area of PR-19 CNFs was somewhat smaller than that of PR-24 CNFs possibly due to the CVD layer present on PR-19 nanofibers, which could cover some of the roughness present in PR-24 fibers. However, we also note that the difference is not very significant given that different batches of PR-19-PS nanofibers have been reported to have a surface area varying from 20.74 m^2/g to 38.02 m^2/g.[13] But, from our results, it is evident that the surface area of MJ CNFs is almost an order of magnitude higher than that of PR CNFs even though these nanofibers have similar diameters. This large surface area is consistent with the significantly rough surface observed from STEM micrographs for MJ fibers (relative to that for PR fibers).

Figure 9(a–h) display TEM micrographs of LLDPE lamellar structure in pure and composite forms (15 wt % of PR-19, PR-24, and MJ CNFs) for two different magnifications. Lamellae growing perpendicular

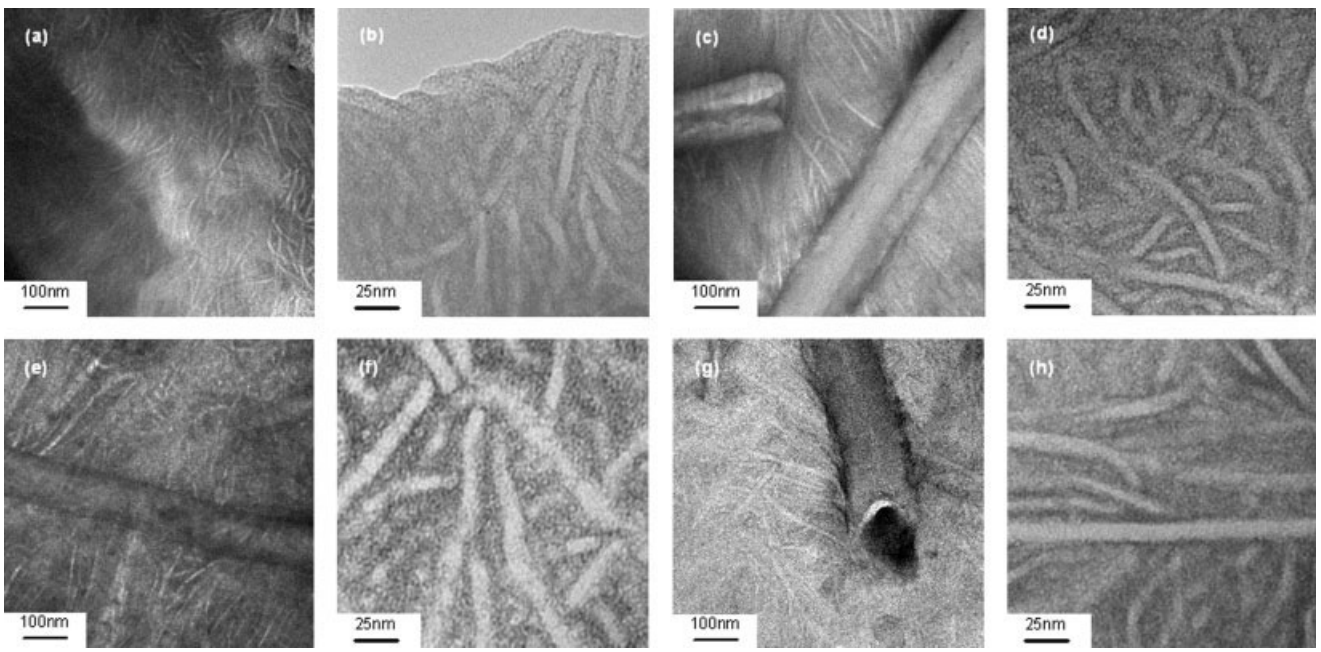

Figure 9 Transmission electron micrographs at two magnification levels for: (a,b) pure LLDPE, and LLDPE/15 wt % nanocomposites containing (c,d) PR-19, (e,f) PR-24 and (g,h) MJ CNFs.

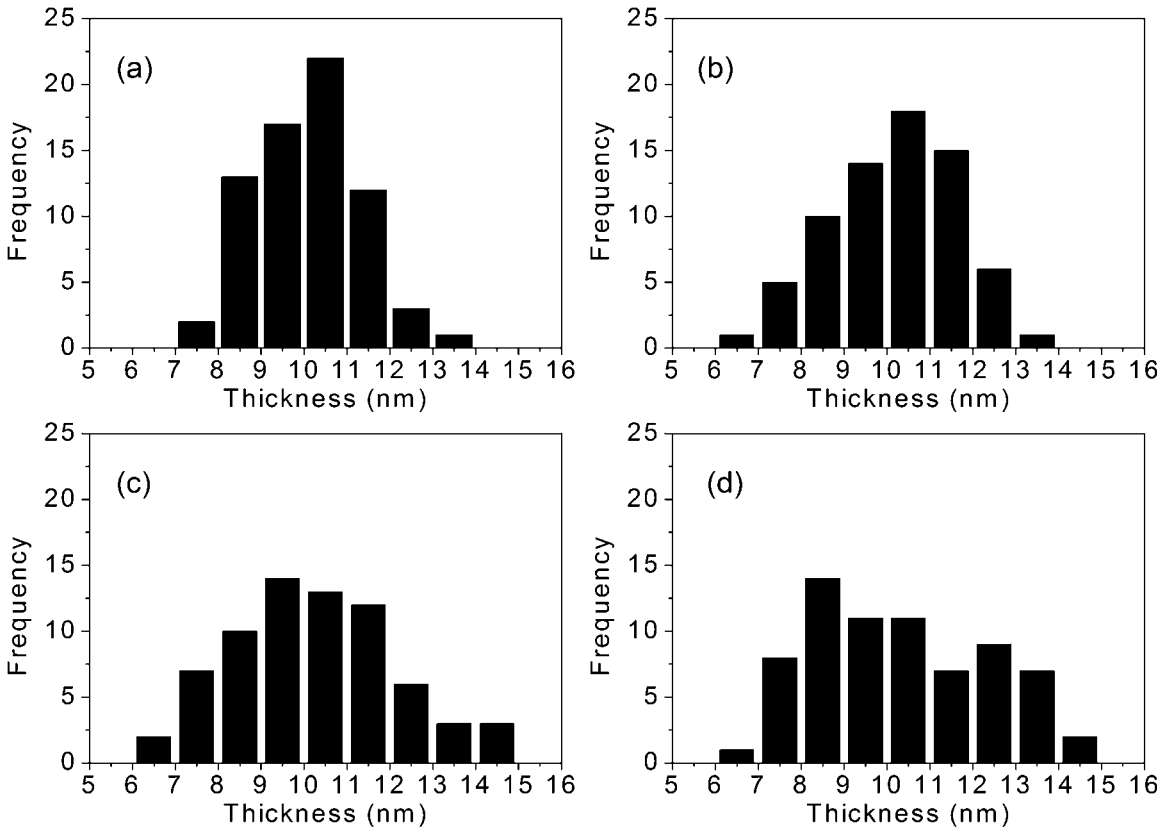

Figure 10 Histograms of thickness distribution of LLDPE lamellae in: (a) pure form, and 15 wt % nanocomposites containing (b) PR-19, (c) PR-24 and (d) MJ CNFs.

to the surface of CNFs were observed in nanocomposites, indicating the presence of transcrystallinity. The nominal thickness of polymer lamellae were 10.0 ± 1.3 nm, 10.2 ± 1.5 nm, 10.3 ± 1.9 nm, and 10.3 ± 2.0 nm for pure LLDPE, PR-19, PR-24, and MJ nanocomposites, respectively. These values were not significantly different in the pure versus nanocomposite form. However, a broader distribution of LLDPE lamellar thickness was observed in nanocomposites compared to that in the pure state [Fig. 10(a–d)]. This is also consistent with results reported by Wu et al.[31] who showed the preferential crystalline growth of HDPE at the end of carbon fibers was a consequence of surface roughness. Therefore, as expected, surface topography of the nanoreinforcement plays an important role in the crystallization behavior of the polymer.

CONCLUSIONS

WAXD results indicate that the crystal structure and overall crystallinity of LLDPE did not change significantly in any of the LLDPE/CNF nanocomposites. Nonisothermal DSC analysis of nanocomposites indicated that 15 wt % PR-19 nanocomposite exhibited three melting peaks, similar to those for pure LLDPE. However, one of the three melting peaks for LLDPE disappeared in the presence of MJ CNFs. Further, the observation that the broad melting peak becomes more intense with increasing MJ CNF content suggests that MJ nanofibers lead to thinner LLDPE lamellae. TEM results of nanocomposites revealed transcrystalline growth of LLDPE on CNF surface, and a slightly broader distribution of lamellar thickness. STEM studies revealed a rougher surface morphology of the MJ nanofibers relative to that of PR nanofibers. BET studies confirmed a larger specific surface area of MJ nanofibers relative to that of PR nanofibers, suggesting that the larger and the rougher surface of MJ nanofibers contributes toward the different crystallization behavior of the nanocomposites.

Any opinions, findings, conclusions, or recommendations expressed in this article are those of the authors and do not necessarily reflect those of the National Science Foundation. The authors acknowledge Dr. Joan S. Hudson and Mr. Amar Kumbhar for their help in conducting TEM experiments, and Dr. A. Naskar for help with initial X-ray measurements.

References

1. Lozano, K.; Barrera, E. V. J Appl Polym Sci 2001, 79, 125.
2. Lozano, K.; Bonilla-Rios, J.; Barrera, E. V. J Appl Polym Sci 2001, 80, 1162.

3. McNally, T.; Pötschke, P.; Halley, P.; Murphy, M.; Martin, D.; Bell, S. E. J.; Brennan, G. P.; Bein, D.; Lemoine, P.; Quinn, J. P. Polymer 2005, 46, 8222.
4. Bhattacharyya, A. R.; Sreekumar, T. V.; Liu, T.; Kumar, S.; Ericson, L. M.; Hauge, R. H.; Smalley, R. E. Polymer 2003, 44, 2373.
5. Manchado, M. A. L.; Valentini, L.; Biagiotti, J.; Kenny, J. M. Carbon 2005, 43, 1499.
6. Probst, O.; Moore, E. M.; Resasco, D. E.; Grady, B. P. Polymer 2004, 45, 4437.
7. Li, S. N.; Li, Z. M.; Yang, M. B.; Hu, Z. Q.; Xu, X. B.; Huang, R. Mater Lett 2004, 58, 3967.
8. Cherukupalli, S. S.; Ogale, A. A. Polym Eng Sci 2004, 44, 1484.
9. Prasad, A. Polym Eng Sci 1998, 38, 1716.
10. Lee, S.; Kim, M. S.; Ogale, A. A. SPE ANTEC Proc 2006, 486.
11. Tibbetts, G. G.; Lake, M. L.; Strong, K. L.; Rice, B. P. Comp Sci Tech 2007, 67, 1709.
12. Uchida, T.; Anderson, D. P.; Minus, M. L.; Kumar, S. J Mater Sci 2006, 41, 5851.
13. Lakshminarayanan, P. V.; Toghiani, H.; Pittman, C. U. Carbon 2004, 42, 2433.
14. Lee, B. O.; Woo, W. J.; Song, H. S.; Park, H. S.; Hahm, H. S.; Wu, J. P.; Kim, M. S. J Ind Eng Chem 2001, 7, 305.
15. Lee, B. O.; Woo, W. J.; Kim, M. S. Macromol Mater Eng 2001, 286, 114.
16. Gregg, S. J.; Sing, K. S. W. Adsorption, Surface Area, and Porosity; Academic Press: New York, 1967; Chapter 2.
17. Sawyer, L. C.; Grubb, D. T. Polymer Microscopy, 2nd ed.; Chapman & Hall: London, 1996; Chapter 4.
18. Defoor, F.; Groeninckx, G.; Schouterden, P.; Van der Heijden, B. Polymer 1992, 33, 5186.
19. Springer, H.; Hengse, A.; Hohne, J.; Schich, A.; Hinrichsen, G. Progr Coll Polym Sci 1986, 72, 101.
20. Schouterden, P.; Groeninckx, G.; Van der Heijden, B.; Jansen, F. Polymer 1987, 28, 2099.
21. Puig, C. C.; Aviles, M. V.; Joskowicz, P.; Diaz, A. J Appl Polym Sci 2001, 79, 2022.
22. Sperling, L. H. Introduction to Physical Polymer Science, 3rd ed.; Wiley: New York, 2001; Chapter 6.
23. Gupta, A. K.; Rana, S. K.; Deopura, B. L. J Appl Polym Sci 1994, 51, 231.
24. Rabesiaka, J.; Kovacs, A. J. J Appl Phys 1961, 32, 2314.
25. Mirabella, F. M.; Bafna, A. J Polym Sci Part B: Polym Phys 2002, 40, 1637.
26. Aggarwall, S. L.; Tilley, G. P. J Polym Sci 1955, 18, 17.
27. Orsini, P. G.; Marchese, B.; Mazzarella, L. J Polym Sci Part A: Gen Pap 1963, 1, 1901.
28. Beach, D. L.; Kissin, Y. V. J Polym Sci 1984, 22, 3027.
29. Feng, L.; Kamal, M. R. Polym Eng Sci 2005, 45, 1140.
30. Janimak, J. J.; Stevens, G. C. Thermochim Acta 1999, 332, 125.
31. Wu, G.; Asai, S.; Sumita, M. Macromolecules 2002, 35, 945.